THE CVD VARIABLES METHOD FOR TAILORING HFCVD CARBON NANOTUBE MORPHOLOGY

Ashfaq Hussain
College of Engineering and Computer Science,
University of Central Florida, Orlando, Florida, United States of America
Department of Mechanical Engineering, University of Malaya, Kuala Lumpur, Malaysia

Abstract

In research on carbon nanotube growth by hot filament chemical vapor deposition (HFCVD), variations of HFCVD have yielded promising results. However, these systems have used plasma enhancement to tailor nanotube morphology. The use of plasma enhancement has made these HFCVD systems expensive to operate and difficult to scale up. This report presents research results to show that it is possible to use the inherent capabilities of variation in CVD parameters like pressure, temperature, and gas composition to tailor nanotube growth in the HFCVD system without resorting to additional cumbersome techniques, thus retaining the value of HFCVD as a low cost and scalable method.

Keywords: Carbon nanotubes, chemical vapor deposition, hot filament, morphology

Introduction

Since the discovery of carbon nanotubes (CNTs) in 1991 [1], they have been found to possess very interesting mechanical, chemical and electrical properties and have been proposed as prime materials for a number of applications. Their property as an excellent field electron emitter has been the basis of their study for applications such as cold cathode flat panel displays and electron guns. A variety of chemical vapor deposition methods have been used to produce carbon nanotube arrays appropriate for field emission applications. Researchers have found that for suitable tailoring of nanotube morphology during chemical vapor deposition of nanotubes for field emission applications, it is necessary to use one or the other of the following procedures: (a) Extensive substrate surface preparation [2-5]. (b) Plasma enhancement combined with HFCVD (PE-HFCVD) [6-14]. These methods, even though they succeed in in-situ growth of good quality carbon nanotubes, are costly and difficult to scale-up. In the case of PE-HFCVD, these two disadvantages accrue to it due to the plasma enhancement part of this method even though HFCVD is inherently a low cost method with scale-up capability. Thus there is a need for using HFCVD for in situ growth of carbon nanotubes in a manner that does not nullify its inherent advantages. In this report, we show that it is possible to meet this objective by controlling the catalyst-assisted growth of carbon nanotubes in HFCVD system purely through variation of CVD parameters like gas composition, pressure and temperature and this variation can therefore be used to tailor the nanotube synthesis. This control in HFCVD depends, as shown here, on the inherent capabilities of changes in CVD variables to modify carbon nanotube morphology during growth.

Experiment

The hot filament chemical vapor deposition (HFCVD) system used for this investigation has been described elsewhere [15]. The HFCVD reaction chamber pressure was varied between 5 and 100 torr. Temperature variation was between 700°C and 950°C. The

composition of the CH_4:H_2:Ar precursor gas mixture was varied in such a way that methane contents of 10, 15, and 20 percent were investigated at increasing hydrogen to argon ratios from 10:80 to 60:30. Chemical vapor deposition was carried out on substrates consisting of vacuum-deposited layers of iron-nickel particles and films on silicon wafers. Scanning electron microscope was used to characterize the results.

Results

The sets of micrographs shown in Figures 1 to 5 show particular instances of some typical results obtained during the investigation of the effects on deposit morphology of change in pressure, temperature, methane content, catalyst density, and H_2:Ar ratio.

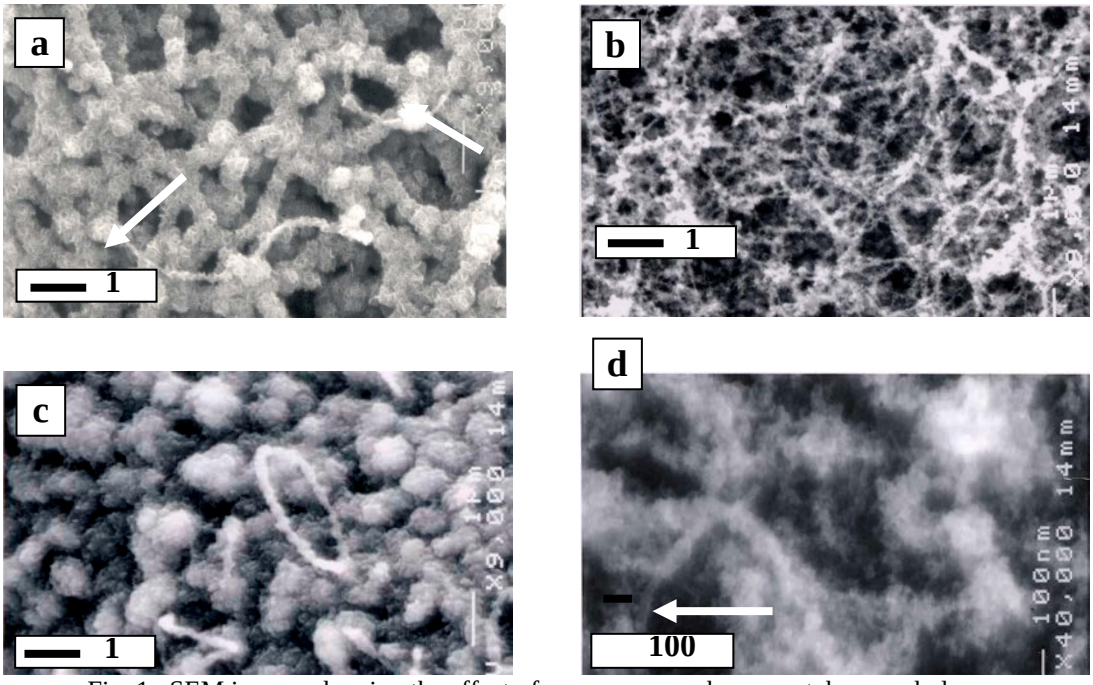

Fig. 1. SEM images showing the effect of pressure on carbon nanotube morphology:
(a) CH_4 content = 10%, Temperature = 700ºC, Pressure = 20 torr, H_2/Ar ratio = 10/80;
(b) CH_4 content = 10%, Temperature = 700ºC, Pressure = 60 torr, H_2/Ar ratio = 10/80;
(c) CH_4 content = 10%, Temperature = 700ºC, Pressure = 100 torr, H_2/Ar ratio = 10/80;
(d) CH_4 content = 10%, Temperature = 700ºC, Pressure = 60 torr, H_2/Ar ratio = 10/80.

Fig. 1a to Fig. 1c shows the effect of change in pressure from 20 to 60 to 100 torr at CH_4:H_2:Ar composition of 10:10:80 and temperature of 700°C. At 20 torr pressure (Fig. 1a), the filamentous nature of the chemical vapor deposit is obvious but the structure is very coarse. Two finer filaments on top of the deposit (indicated by arrows) suggest that the coarse filaments have grown by graphite flake accumulation from narrower cores arising from the catalyst particles. Increasing the pressure to 60 torr (Fig. 1b) refines the filamentous structure. Examination of the high magnification micrograph at this pressure (Fig. 1d) reveals the nanotubular cores of the fibers at this pressure (indicated by the arrow in Fig. 1d), which appear to be overladen with amorphous carbon deposit. A further increase in pressure to 100 torr gives a deposit with very few fibers and a dense graphitic growth over catalyst particles.

Fig. 2a to Fig. 2c shows the effect of change on microstructure in methane content from 10 to 15 to 20 percent at temperature of 900°C, pressure of 80 torr and hydrogen to argon ratio of 40/50. At 10 percent methane (Fig. 2a) there is not enough carbon deposition to saturate the catalyst particles and cause nanotube formation. 15 percent methane (Fig. 2b) causes formation of nanotubes which are in various stages of nucleation and growth but have a uniform diameter of about 100 nm. Finally at 20 percent methane content (Fig. 2c) the carbon deposition is too high to allow nucleation of nanotubes.

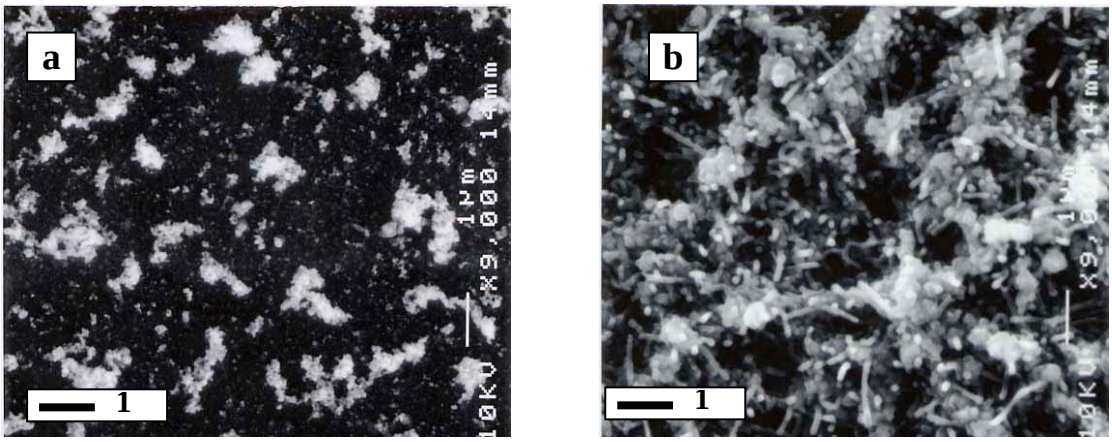

Fig. 2. SEM images showing the effect of methane content on carbon nanotube morphology:
(a) CH_4 content = 10%, Temperature = 900ºC, Pressure = 80 torr, H_2/Ar ratio = 40/50;
(b) CH_4 content = 15%, Temperature =900ºC, Pressure = 80 torr, H_2/Ar ratio = 40/50;
(c) CH_4 content = 20%, Temperature = 900ºC, Pressure = 80 torr, H_2/Ar ratio = 40/50.

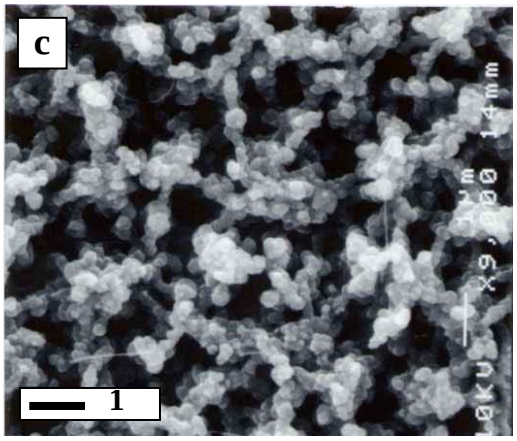

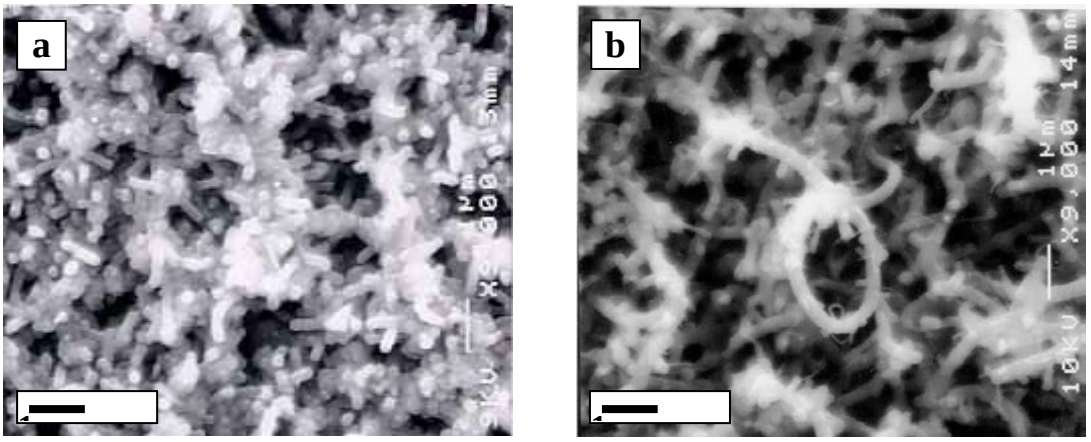

Fig. 3. SEM images showing the effect of temperature on carbon nanotube morphology:
(a) CH_4 content = 20%, Temperature = 900ºC, Pressure = 60 torr, H_2/Ar ratio = 30/60;
(b) CH_4 content = 20%, Temperature = 950ºC, Pressure = 60 torr, H_2/Ar ratio = 30/60.

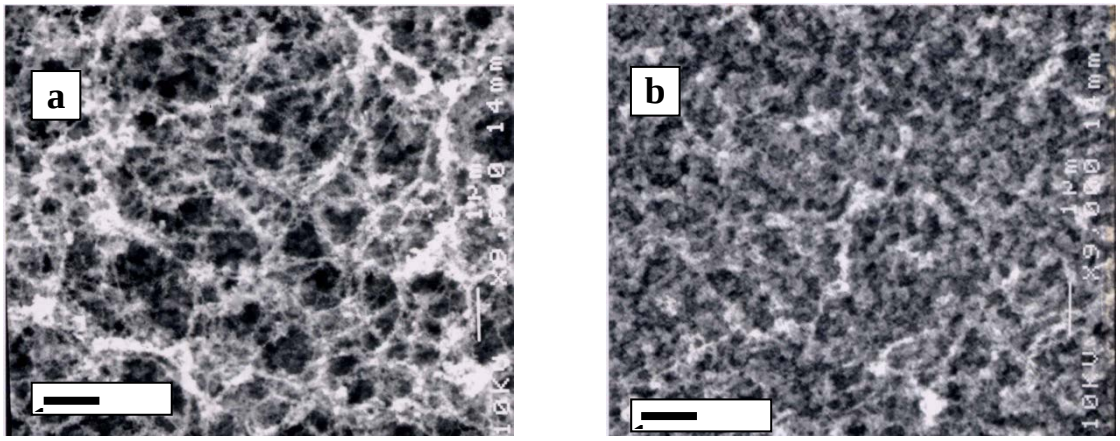

Fig. 4. SEM images showing the effect of temperature on carbon nanotube morphology:
(a) CH_4 content = 20%, Temperature = 900ºC, Pressure = 60 torr, H_2/Ar ratio = 30/60;
(b) CH_4 content = 20%, Temperature = 900ºC, Pressure = 60 torr, H_2/Ar ratio = 30/60.

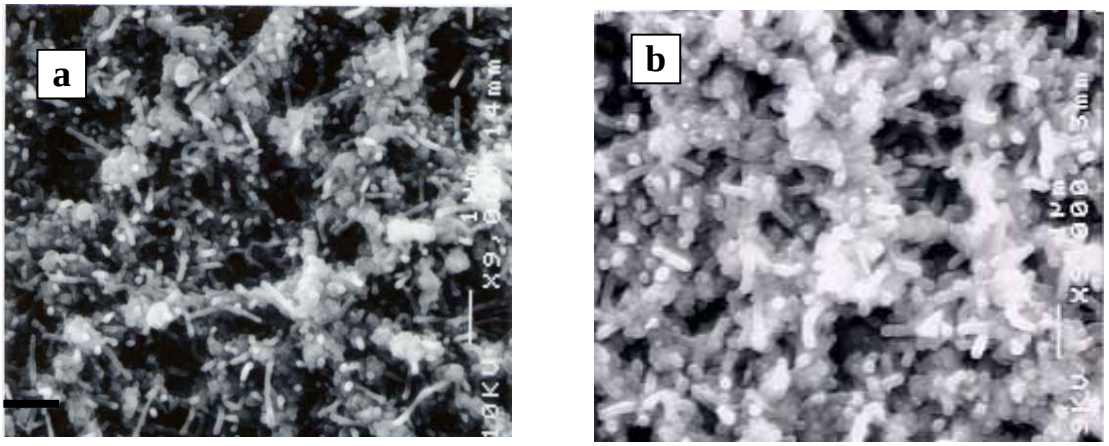

Fig. 5. SEM images showing the effect of H_2/Ar ratio on carbon nanotube morphology:
(a) CH_4 content = 15%, Temperature = 900ºC, Pressure = 80 torr, H_2/Ar ratio = 40/50;
(b) CH_4 content = 15%, Temperature = 900ºC, Pressure = 80 torr, H_2/Ar ratio = 50/40, Magnification = X9,000;
(c) Same CVD conditions as in (b) at a magnification of X1,000.

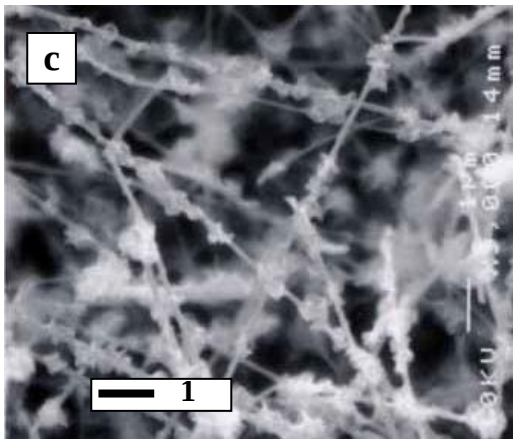

The effect of change in temperature is disclosed in Fig. 3. As the temperature is increased from 900 to 950°C (Fig. 3a to Fig. 3b) at 15 percent methane content, 60 torr pressure, and hydrogen to argon ratio of 30/60, it is found that there is a spurt in thickness and growth of nanotubes from the lower to the higher temperature.

Typical effect of change in catalyst density and thickness is represented by the transition shown in Fig. 4a to Fig. 4b from Fe-Ni particle density to Fe-Ni layer density at 20 percent methane content, hydrogen to argon ratio of 30/60, temperature of 900°C, and pressure of 60 torr. The thickness of nanotubes in Fig. 4b is about twice that of nanotubes in

Fig. 4a but there is no change in their length. This is unlike the change in nanotube morphology due to temperature increase where both thickness and length had increased.

Regarding the effect of a change in hydrogen to argon ratio, it was found that an increase in this ratio, resulting in an increase in atomic hydrogen etching effect, would deteriorate an already fine fibrous structure (as shown in the change from 10/80 to 30/60 of this value in Fig. 6a to Fig. 6b at 10 percent methane content, 700°C temperature and 60 torr pressure) but would enhance tubular growth if it had the effect of etching away excess graphitic layers on top of growing nanotubes (as shown in the transition from 40/50 to 50/40 of hydrogen to argon ratio in Fig. 5a to Fig. 5b-c at 15 percent methane, 900°C temperature, and 80 torr pressure).

Discussion

In the pressure effect sequence (Fig. 1), the nanotubes forming the cores of the fibrous structures at 20 and 60 torr pressures have the same thickness, around 40 to 50 nm. What differenciates the two structures is the manner in which carbon deposition occurs over these core nanotubes in the two cases. Under nanotube growth promoting conditions the nanotubes increase in thickness by addition of graphitic walls to their structure at the same time as their length increases, even though increase in the former dimension is more gradual than the latter. The process of wall addition depends on diffusion and precipitation of carbon around the nanotubes and is highly temperature and pressure dependent. There is evidence that in the pressure range between 10 and 50 torr, as the deposition temperature is lowered below 1600°C, there is substantial increase in interlayer spacing of deposited graphite [16]. At temperature of 700°C and 20 torr pressure graphite can only form around the nanotube cores in the form of widely spaced, crumpled, and overlapping flakes, resulting in the coarse filaments observed. Increase in pressure to 60 torr at the same temperature prevents graphite formation from the deposited carbon and accumulation of amorphous carbon around the cores results, giving finer filaments than at 20 torr. Pressure of 100 torr causes deposited carbon to form dense graphitic growth over catalyst particles, suppressing most nanotube growth and resulting in a hillock-type structure.

Methane in the precursor gas mixture has to undergo dissociation before the released carbon species can dissolve into catalyst metal and reappear as crystalline graphite upon saturation. At a relatively low level of methane content, only enough carbon is processed to lead to growth of some graphitic layers on catalyst particles (Fig. 2a). As the methane content is raised, the rate of carbon being processed into graphitic layers is increased so that the number of graphitic layers reaches the target necessary for nucleation and growth of nanotubes (Fig. 2b). If the methane content is raised upto a level where the rate of carbon being deposited is beyond the absorption capacity of catalyst particles, the excess carbon will begin to accumulate as amorphous carbon (Fig. 2c), a process which has also been called ‘carbonization’, as opposed to the process of graphitic layer formation known as graphitization. Even though catalyst particles are mostly covered with amorphous carbon at this methane content, the process of graphitization is seen not to stop completely. As disclosed in Fig. 2c, graphitization and nanotube formation may still take place over small uncovered catalyst particle surfaces where the combination of appropriate graphitization level and catalyst metal grain size will satisfy the nanotube nucleation and growth requirements, giving rise to a thin population of fine nanotubes. From the uniformity in thickness of these

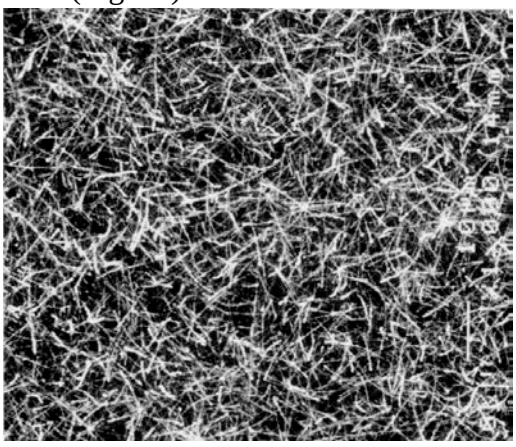

fine nanotubes it can be inferred that there is a unique combination of graphitization level and grain size under the given set of conditions which is giving rise to these nanotubes.

The general increase in thickness and length of nanotubes with increase in temperature (Fig. 3) can be understood in terms of the effects that temperature increase will have on growth conditions. Major effects of the temperature increase include: (a) Greater solubility of carbon in Fe-Ni catalyst particles. (b) Increase in diffusion of carbon atoms within and on the surface of catalyst particles. (c) Increase in the rate of graphitization because of effects (a) and (b). (d) Increase in plasticity of catalyst metal particles. The average nanotube thickness is around 160 nm at 900°C (Fig. 3a) and 230 nm at 950°C

(Fig. 3b). Carbon solubility limits in 50:50 Fe-Ni at 900°C and 950°C are approximately 0.15 wt% and 0.20 wt% respectively [17]. There appears to be a close correlation between the proportion of nanotube thickness increase and increase of carbon solubility in Fe-Ni with increase in temperature. The increase in graphitization resulting from greater C solubility at higher temperatures will render larger grains suitable for nanotube formation because greater number of graphitic layers covering these grains will possess the increased combined elastic stress required for this formation. The increase in plasticity of the catalyst particles with increasing temperature would enhance this effect. Thus, thicker nanotubes will result at higher temperatures.

The change in nanotube morphology due to change in catalyst density (Fig. 4a to Fig. 4b) appears to have resulted from difference in grain size and carbon absorption capacity between the catalyst particle layer and catalyst film layer. The low density particle layer with lower absorption capacity and smaller grain size will have lower graphitization and thinner nanotubes as opposed to the film layer which has greater density and absorption capacity and will give rise to higher graphitization and thicker nanotubes. As noted in the results section, the catalyst density increase effect increases the thickness of nanotubes but not their length whereas the temperature increase effect increases both the thickness and length of nanotubes. The reason for this difference lies in the fact that catalyst density increase enhances only the absorption of carbon into catalyst metal but temperature increase enhances both absorption of carbon atoms into catalyst metal as well as their diffusion.

The etching effect of atomic hydrogen produced by dissociation of hydrogen gas at the tungsten filament and the dilution of this etching effect by argon gas are the two opposing effects represented by the variation in hydrogen to argon ratio. How this etching effect interacts with graphitic layers on catalyst particles determines how hydrogen to argon ratio affects nanotube growth. According to the generally accepted nanotube growth mechanism, a certain number of graphitic layers around a grain will have just enough elastic stress to force a cylindrical shape on both the graphitic layers and the catalyst grain, giving rise to nanotube nucleation. If the number of graphitic layers is less than this threshold number, not enough stress will exist for nanotube nucleation whereas build-up of graphitic layers above that limit will require growth of nanotubes thicker than could be justified by availability of graphite recrystallizing from the catalyst metal. Increase in hydrogen to argon ratio will have the effect of etching out graphitic layers, thus allowing nanotube growth in the latter case (Fig. 5a to Fig. 5b). In case where nanotubes of fine dimensions pre-exist in the microstructure, an increase in hydrogen to argon ratio will wipe them out (Fig. 6a to Fig. 6b). The evolution of a rich, smooth-walled and uniform-diameter growth of nanotubes after adjustment of H_2/Ar ratio in Fig. 5b (Fig. 5c is another view of this structure at a different magnification) from the microstructure in Fig. 5a which itself resulted from adjustments in CVD variables, represents a clear case of using the inherent capabilities of CVD parameter variation to promote nanotube growth unaided by any other technique.

Conclusion

Systematic variation of CH_4-H_2-Ar gas mixture composition, pressure, temperature, and substrate catalyst density were carried out in a hot filament chemical vapor deposition (HFCVD) system on Fe-Ni deposited silicon substrates to find the role of these variables on carbon nanotube growth morphology. The following nanotube-tailoring effects were found: (a) Increase in pressure in general could be used to improve nanotube formation but pressures above 90 torr tended to wipe out nanostructural features. (b) Increase in methane content under the right conditions could be used to supply carbon for nanotube formation and speed up their growth but beyond that limit would kill tubular formation. (c) Increase or decrease in temperature could be used to accelerate or decelerate growth and thickness of nanotubes. (d) Change in catalyst layer density could be used to change the nanotube diameter. (e) Increase in etching effect represented by the increase in H_2/Ar ratio could be used to promote nanotube growth in those cases where the etching effect released tube nuclei from overlayers of material stunting their growth but the increase of this ratio could also be used to etch out existing fine nanofeatures where necessary. The application of the etching effect principle shown in Fig. 5a-c resulted in a dense growth of smooth-walled, uniform-diameter nanotubes.

We thus conclude that the variation of CVD parameters offers us a rich assortment of effects which can be used to tailor the nanotube morphology in the HFCVD system quite independent of the use of additional techniques like plasma enhancement which make HFCVD costly and difficult to scale up.

References:

S. Ijima: Nature Vol. 354 (1991), p. 56.
W.Z. Li, S.S. Xie, L.X. Qian, B.H. Chang, B.S. Zhou, W.Y. Zhou, R.A. Zhao and G. Wang: Science Vol. 274 (1996), p. 1701.
M. Terrones, N. Grobert, J. Olivarres, J.P. Zhang, H. Terrones, K. Kordatos, W.K. Hsu, J.P. Hare, P.D. Townsend, K Prassides, A.K. Cheetham, H.W. Kroto and D.R.M. Walton: Nature Vol. 388 (1997), p. 52.
G.L. Che, B.B. Lakshmi, E.R. Fisher and C.R. Martin: Nature Vol. 393 (1998), p. 346.
S. Fan, M.G. Chapline, N.R. Franklin, T.W. Tombler, A.M. Cassell and H. Dai: Science Vol. 283 (1999), p. 512.
Y. Chen, D.T. Shaw and L. Guo: Appl. Phys. Lett. Vol. 76 (2000), p. 2469.
F. Ren, Z.P. Huang, J.W. Xu, J.H. Wang, P. Bush, M.P. Siegal and P.N. Provencio: Science Vol. 282 (1998), p. 1105.
Z.P. Huang, J.W. Xu, Z.F. Ren, J.H. Wang, M.P. Siegal and P.N. Provencio: Appl. Phys. Lett. Vol. 73 (1998), p. 3845.
Z.F. Ren, Z.P. Huang, D.Z. Wang, J.G. Wen, J.W. Xu, J.H. Wang, L.E. Calvet, J. Chen, J.F. Klemic and M.A. Reed: Appl. Phys. Lett. Vol. 75 (1999), p. 1086.
Y. Chen, L. Guo, S. Patel and D.T. Shaw: J. Mater. Sci. Vol. 35 (2000), p. 5517.
J. Yu, X.D. Bai, J. Ahn, S.F. Yoon, E.G. Wang: Chem. Phys. Lett. Vol. 323 (2000), p. 529.